Performance Evaluation of Local Gabor Wavelet-based Disparity Map Computation

M.K. Bhuyan and Malathi. T
Department of Electronics and Electrical Engineering,
Indian Institute of Technology Guwahati, India-781039.
E-mail: (mkb, malathi) @iitg.ernet.in

ABSTRACT

Stereo correspondence aims to find the matching pixels which are from the same real world point from the stereo images. It finds applications in 3D reconstruction, video surveillance and object recognition. In the last few decades, a lot of work is done in disparity map estimation which is either in the matching cost computation i.e., new features are proposed for matching purpose or in cost aggregation. In addition to this, progress is also done in the disparity refinement step also. The maximum performance of the estimated disparity map depends on fine tuning the various parameter values used. In this paper, we evaluate the impact of the various parameters of the proposed method on the estimated disparity map. The proposed method uses Gabor wavelet-based feature for matching cost computation. Experimental results show the impact of various parameters in the estimated disparity map. Error is evaluated in three regions of the disparity map namely – non-occluded, all and discontinuous regions.

KEYWORDS

Feature extraction, Gabor filter, Kuwahara filter, Cost aggregation, disparity map

1 INTRODUCTION

Stereo correspondence is an important research topic in computer vision and active for more than a decade finding application in image rendering, robotics and surveillance. Most stereo correspondence methods can be categorized into the following four steps - Matching cost computation, cost aggregation, disparity computation and disparity refinement [1]. Based on the approach used for disparity computation, stereo correspondence methods can be classified into local or global. Local method uses winner-take-all (WTA) approach for disparity computation whereas global method uses optimization.

Stereo correspondence methods can be broadly classified into local, global and semi-global methods. Global methods are formulated as an energy-minimization problem, where the main objective is to find a disparity function that minimizes a global energy [2]. Graph cut, Dynamic programming are the most commonly used optimization methods. On the other hand, local stereo matching algorithms have uniform structure and can be parallelized [3]. In these methods, it is not required to search all the pixels of one image to find a best match of a particular pixel in the other image i.e., matching of a particular pixel does not influence the matching of its neighboring pixels. Semi-global algorithms combine the concept of both the local and the global algorithms, which are relatively less complex [4].

2 RELATED WORKS

The basic matching cost function used in stereo correspondence are sum of absolute difference (SAD), sum of squared difference (SSD) and normalized cross correlation (NCC) [5]. In addition to this, nonparametric transforms such as rank and census transform [6], mutual information [4] and permeability [7] are also used for matching cost computation. Table 1

Table 1. LOCAL STEREO MATCHING APPROACHES

Matching Metrics	Matching Expressions
SAD	$\sum_{p,q\in N} \lvert I_L(p,q) - I_R(p-d,q)\rvert$
SSD	$\sum_{p,q\in N} \left(I_L(p,q) - I_R(p-d,q)\right)^2$
NCC	$\dfrac{\sum_{p,q\in N} \left(I_L(p,q)-\bar{I}_L\right)-\left(I_R(p-d,q)-\bar{I}_R\right)}{\sqrt{\sum_{p,q\in N} \left(I_L(p,q)-\bar{I}_L\right)^2-\left(I_R(p-d,q)-\bar{I}_R\right)^2}}$
Rank	$\sum_{p,q\in N} \left(I_L'(p,q) - I_R'(p-d,q)\right)$ $I_L'(p,q) = \sum_{u,v\in W} I_l(u,v) < I_l(p,q)$
Census	$\sum_{p,q\in N} HAMMING\left(I_L'(p,q), I_R'(p-d,q)\right)$ $I_L'(p,q) = \underset{u,v}{BITSTRING}\left(I_l(u,v) < I_l(p,q)\right)$

shows the expressions of few matching function used to find the matching cost. After the introduction of adaptive support weights, the performances of local methods are comparable to those generated by global methods. First and foremost adaptive support weight was proposed by Yoon and Kweon [8,9]. In this method, weights are assigned to the pixels within the correlation window based on gestalt grouping. The support weight of a pixel can be written as

$$w(i,j) = f\left(\Delta c_{ij}, \Delta g_{ij}\right) = f_s\left(\Delta c_{ij}\right) f_p\left(\Delta g_{ij}\right) \quad (1)$$

where, $f_s\left(\Delta c_{ij}\right)$ and $f_p\left(\Delta g_{ij}\right)$ represents the strength of grouping by color similarity and spatial proximity, respectively. $f_s\left(\Delta c_{ij}\right)$ and $f_p\left(\Delta g_{ij}\right)$ are inversely proportional to the color dissimilarity and spatial distance from the center pixel, respectively. The strength of grouping by color similarity is defined as

$$f_s\left(\Delta c_{ij}\right) = \exp\left(\frac{-\Delta c_{ij}}{\gamma_c}\right) \quad (2)$$

Here, Δc_{ij} denotes the color dissimilarity between two pixels in the CIELab color space. The strength of grouping by proximity is defined as

$$f_p\left(\Delta g_{ij}\right) = \exp\left(\frac{-\Delta g_{ij}}{\gamma_p}\right) \quad (3)$$

where, Δg_{ij} is the spatial distance of two pixels in the image domain. Hence,

$$w(i,j) = \exp\left(-\left(\frac{\Delta c_{ij}}{\gamma_c} + \frac{\Delta g_{ij}}{\gamma_p}\right)\right) \quad (4)$$

These weights are similar to the weights based on bilateral filter. Gerrits [10] proposed weight computing method which depends on the precomputed mean-shift color segmentation. Pixels belonging to the same segment as the center pixels are assigned weight 1 whereas pixels in other segments are given weight 0. This method suffers from computational complexity due to mean-shift segmentation. Hosni et al computed weight that relies on the geodesic distance from the center pixel [11]. In this method, pixels having approximately constant color path to the center pixel are assigned high weight. Zhang et al allowed multi scale for cost aggregation [12]. This cross-scale cost aggregation framework introduces inter-scale regularizer into the optimization technique. They have integrated various cost aggregation into this framework and shown this leads to significant improvement in the performance. To tackle window size problem, Zhang et al proposed a cross shaped support arms with varying lengths [13]. First, cross shaped support region of varying lengths is constructed based on color similarity and connectivity constraints. Secondly, based on the above decision, a shape adaptive support region is constructed. The proposed orthogonal integral image (OII) technique is the integration of two orthogonal 1-D cost aggregations. A novel information permeability filtering approach is presented for local stereo matching problem [14]. Here, aggregation is done by utilizing separable filtering i.e., performing filtering in horizontal direction and then in the

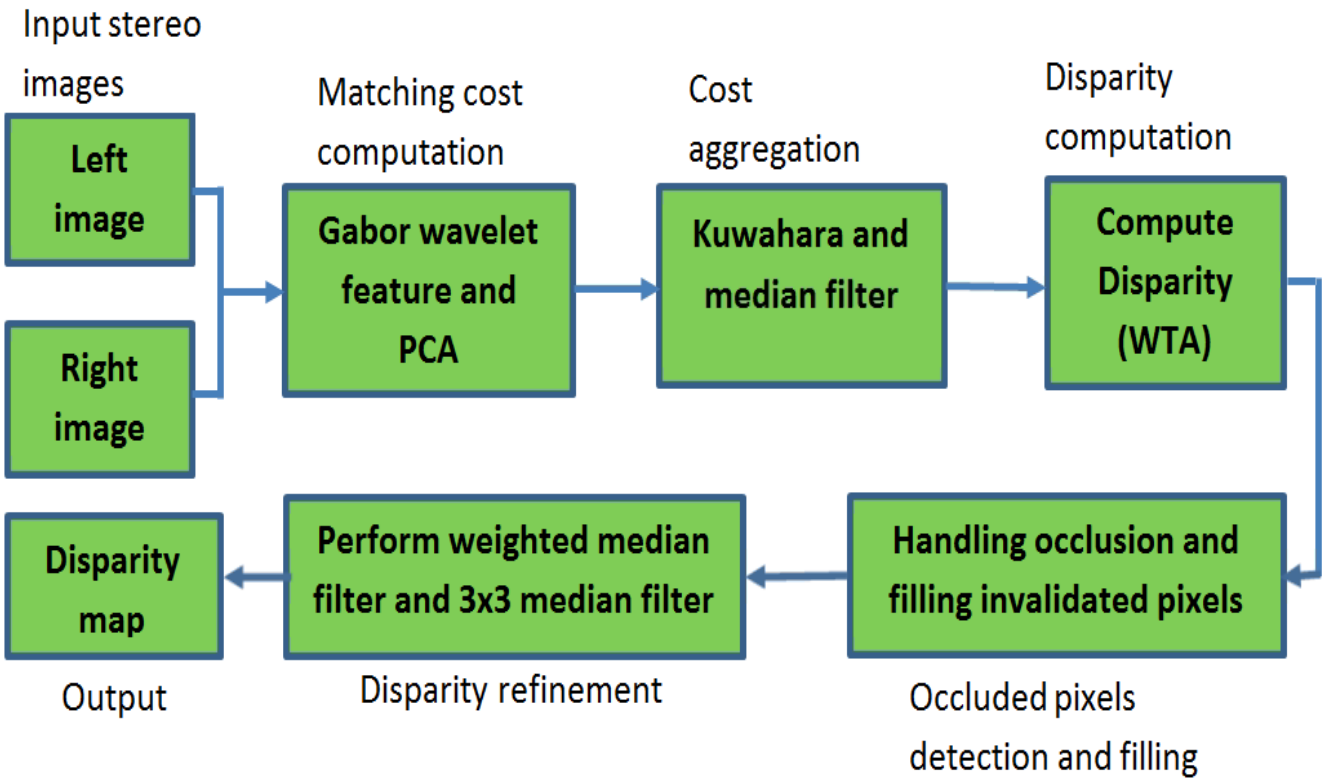

Figure 1. Block diagram of the proposed disparity map computation method.

vertical direction. Rhemann et al made use of guided filter for cost aggregation [15]. The edge preserving property and implementation in linear time i.e., independent of the filter kernel size helps to run the stereo algorithm at real-time frame rates. Min et al proposed joint histogram-based cost aggregation [16]. This method proposed a new representation of likelihood function for cost aggregation which reduces the computational complexity. Sampling scheme inside the matching window greatly reduces the computational complexity of window-based filtering. Pham and Jeon integrate the dimensionality reduction technique, domain transformation into cost aggregation framework [17]. The geodesic distance computed from the transformed domain is used to achieve cost aggregation by performing a sequence of 1-D operations.

The main contributions in this paper are as follows:

- ✓ Local features for matching cost computation are extracted using local Gabor wavelet.
- ✓ Cascaded Kuwahara and median filters are used for cost aggregation.
- ✓ The impact of various parameters such as various window size, number of principal components, Gabor wavelet filter orientations and Gabor wavelet filter scaling on the performance of estimated disparity map is analyzed.

This paper is organized as follows: Section 3 describes in detail the proposed stereo correspondence method, Section 4 shows the experimental results and finally, conclusion in Section 5.

ISBN: 978-1-9491968-07-9 ©2015 SDIWC

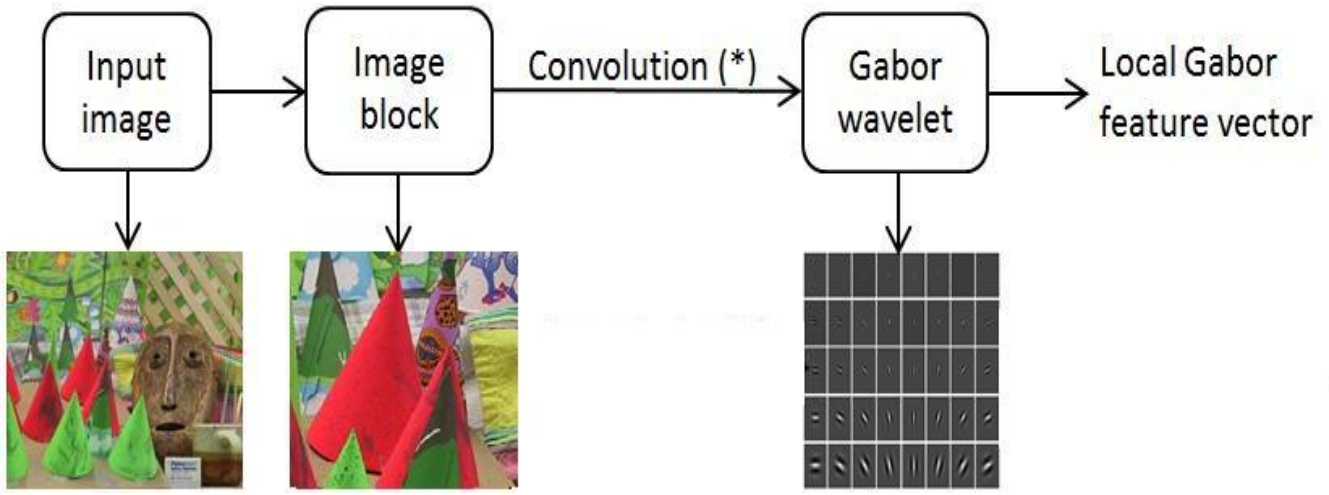

Figure 2. Block diagram of the proposed local Gabor feature extraction.

3 PROPOSED METHOD

Most of the existing stereo matching methods have the following four steps namely - (i) Matching cost computation, (ii) Cost aggregation, (iii) Disparity map computation and (iv) Disparity refinement. The proposed method also follows the above steps. In short, we can describe the proposed method as follows: Local Gabor wavelet features reduced by principal component analysis (PCA) is used to accomplish matching cost computation, Kuwahara and median filter performs cost aggregation, disparity map is computed by winner-take-all (WTA) techniques and finally, occlusion detection and filling followed by disparity refinement shown in Figure 1. All these steps are described in detail in the remaining part of this section.

Matching cost computation: To find the matching cost, feature of the pixel in the left image is compared with the feature of the corresponding pixel in the right image for maximum allowable disparity values. Feature may be intensity, color or texture. Here, we use Gabor wavelet to extract local features. Gabor wavelet is a widely used feature extraction tool in many computer vision applications. The motivation behind using Gabor wavelet for feature extraction is as follows [18]:

- Simple cells in the visual cortex of mammalian brains can be best modeled by Gabor function.
- Gabor wavelet is a bandpass filter and it is an optimal conjoint representation of images in both space and frequency domain that occupies the minimum area.
- The orientation and scale tunable property of Gabor wavelet helps in detecting edge and bars which aids in texture feature extraction [19].
- 2D Gabor wavelet has good spatial localization, orientation selectivity and frequency selectivity property.
- Image perception by human visual system is similar to image analysis by Gabor function.

Gabor functions are Gaussian modulated complex sinusoids given by [20]

$$g(x,y)=\frac{1}{\sqrt{2\pi}}e^{-\frac{1}{8}\left(4x^2+y^2\right)}\left[e^{i\kappa x}-e^{-\frac{k^2}{2}}\right] \qquad (5)$$

Gabor wavelet is referred as a class of self-similar functions generated by the process of orientation and the scaling of the 2D Gabor function given by

$$g_{mn}(x,y) = a^{-m} g(x_a, y_a), a > 1$$
$$x_a = a^{-m}(x\cos\theta + y\sin\theta) \text{ and}$$
$$x_a = a^{-m}(-x\sin\theta + y\cos\theta) \quad (6)$$

where, $\theta = \frac{n\pi}{k}$, m and n are two integers and k is the total number of orientations.

Figure 2 shows the block diagram of the proposed feature extraction method. Consider an image I of size $P \times Q$. In order to find the feature vector for the pixel $I(i, j)$, a certain neighborhood $N(i, j)$ of size $u \times v$ is considered where (i, j) is the pixel coordinates. This patch is convolved with the Gabor filter kernel g_{mn} for different orientations and scaling. Gabor wavelet is a complex filter and here we have used only the real part of Gabor filter for feature extraction. The features are then extracted by concatenating the obtained coefficients given by

$$F(i, j) = concat(\gamma_{mn}(i, j))$$
$$\gamma_{mn}(i, j) = N(i, j) * real(g_{mn}) \quad (7)$$

where, $*$ is the convolution operation and *concat* denotes the concatenation operation. This procedure is repeated for all the pixels in the image. The dimensionality of the obtained features is reduced by PCA [21]. Figure 3 shows the extracted feature for the teddy image. Matching cost is computed by comparing the pixels in the left image with the pixels in the right image along the horizontal line for all possible disparity values. The more similar the pixels are, the lesser is the cost value. Matching cost is a 3D volume with cost values for all pixels at different disparity values.

Cost aggregation: Cost aggregation is the process of smoothing or averaging of computed matching cost for a particular disparity value. In the proposed method we have used cascaded Kuwahara [22] and median filter for cost aggregation. Figure 4 shows the block diagram of the proposed cost aggregation framework. Edge preserving property and run time of $O(1)$ makes Kuwahara filter suitable for cost aggregation. Median filter is used to remove the blocking artifacts produced by Kuwahara filter.

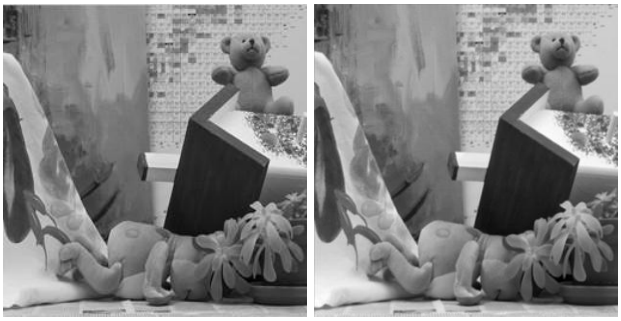

Figure 3. Gabor extracted features. (a) input teddy image and (b) extracted real image.

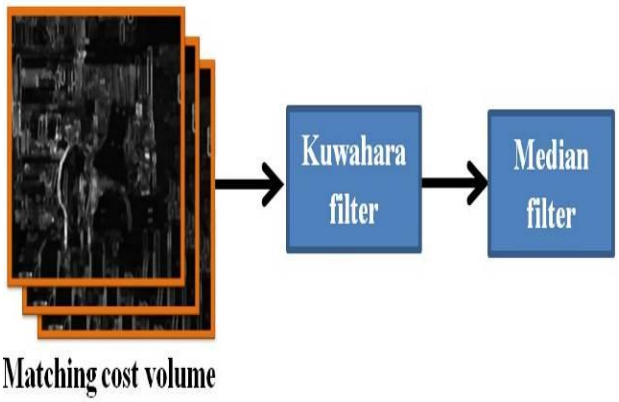

Figure 4. Block diagram of the proposed cost aggregation framework.

Kuwahara filter performs smoothing by dividing the neighborhood of length $2a$ for each pixel into four subregions namely Region 1 (Q_1), Region 2 (Q_2), Region 3 (Q_3) and Region 4 (Q_4) as shown in Figure 5 which is given by

$$\begin{cases} Q_1(i,j) = [i, i+a] \times [j, j+a] \\ Q_2(i,j) = [i-a, i] \times [j, j+a] \\ Q_3(i,j) = [i-a, i] \times [j-a, j] \\ Q_4(i,j) = [i, i+a] \times [j-a, j] \end{cases} \quad (8)$$

where the symbol "×" denotes the Cartesian product.

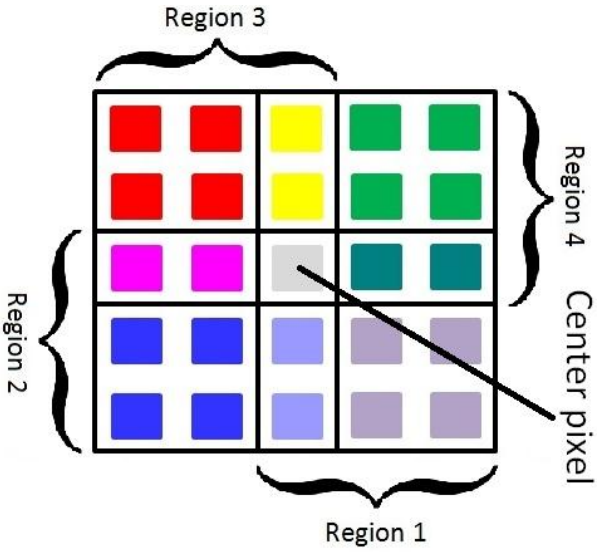

Figure 5. Kuwahara filter subregions.

Local mean $m_z(i,j)$ and variance $\sigma_z(i,j)$ are computed for each subregion $Q_z, z = 1, \cdots, 4$. The mean of the subregion which has minimum variance among the four is assigned to the center pixel (i,j) formulated as

$$\Phi(i,j) = \sum_z m_z(i,j)\, f_z(i,j) \quad (9)$$

where

$$f_z(i,j) = \begin{cases} 1, & \sigma_z(i,j) = \min_k \{\sigma_k(i,j)\} \\ 0, & otherwise \end{cases}$$

Figure 6 shows cost aggregation of cones image. Matching cost of cones image for d=30 is shown in Figure 6(a). Figure 6(b) and (c) shows the matching cost (Figure 6(a)) filtered by Kuwahara filter and followed by median filter, respectively.

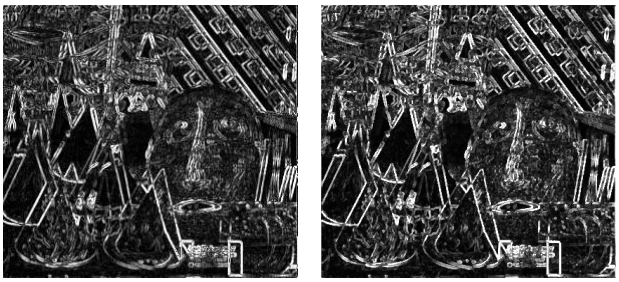

(a) (b)

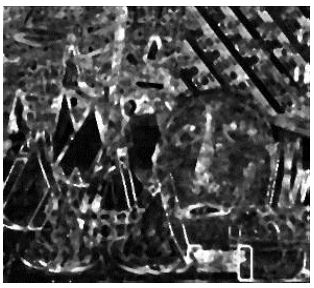

(c)

Figure 6. Cost aggregation of cones stereo images. (a) matching cost (d=30), (b) cost aggregation of (a) by Kuwahara filter and (c) cost aggregation (b) by median filter.

Disparity computation: The disparity map is obtained by determining the disparity d_u of all the pixels $u = (i,j)$ in the reference image. This is accomplished by taking the index of the minimum value in the aggregated cost of the corresponding pixel. Mathematically, the disparity d_u of a pixel u is given by [23]

$$d_u = \arg \min_{d \in D} CA(u,d) \quad (10)$$

where, $CA(u,d)$ is the aggregated matching cost of a pixel u at the disparity d. Here, D denotes the set of allowed disparity values.

Disparity refinement: Occluded pixels are filtered out by the left-right consistency check i.e., another disparity map is extracted by keeping the right image as the reference image.

ISBN: 978-1-9491968-07-9 ©2015 SDIWC

Subsequently, pixels in the left disparity map are compared with the corresponding matching points in the right disparity map. Apparently, it is done to check whether both the disparity maps carry the same disparity value. If the test fails, then the particular pixel is marked as occluded. In occlusion filling step, the disparity d_u of the occluded pixel u is assigned a value of $\min(d_l, d_r)$, where d_l and d_r are the first valid left and right neighbors of the pixel u. Disparity refinement is performed by a constant time weighted median filter [24]. The weights are calculated by the guided image filter. The weights $W(i, j)$ are given by

$$W(i,j) = \frac{1}{\left|\omega^2\right|} \sum_{\kappa:(i,j)\in\omega_\kappa} \left(1 + \left(I_i - \mu_\kappa\right)^T \left(\sum_\kappa + \varepsilon U\right)^{-1} \left(I_j - \mu_\kappa\right)\right) \quad (11)$$

where I_i, I_j and μ_κ are 3×1 vectors. The covariance matrix $\sum_\kappa$ and the identity matrix U have a size of 3×3. Again, $|\omega|$ denotes the number of pixels in the window ω_κ and ε is a smoothness parameter.

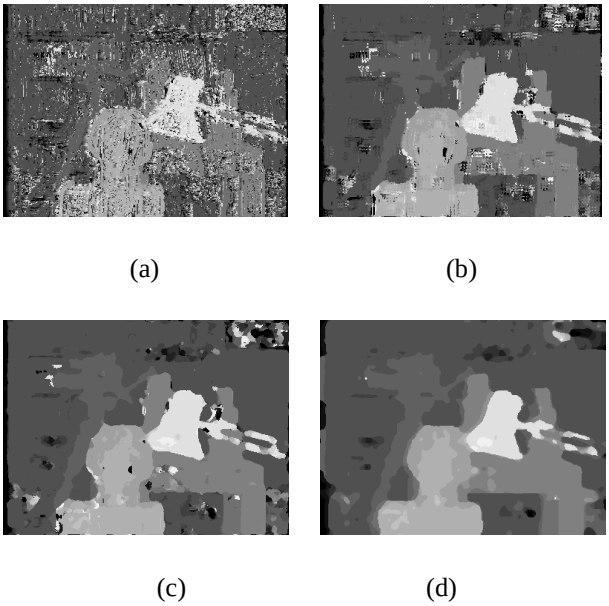

(a) (b)

(c) (d)

Figure 7. Intermediate results. (a) Disparity map from matching cost, (b) disparity map after cost aggregation by only Kuwahara filter, (c) disparity map after cost aggregation using both Kuwahara and median filter (before refinement) and (d) disparity map after refinement.

Figure 7 shows the output at intermediate stage of the proposed disparity map computation method. Important steps of the proposed stereo matching method are shown in Algorithm 1.

Algorithm for disparity map computation

1. Matching cost computation

1.1 Small patch is convolved with the real of the Gabor filter with different orientations and scaling using Eq. (6&7).

1.2 Concatenate the coefficients to obtain the feature shown in Eq. (7).

1.3 Using extracted features, compute matching cost for all possible disparity values.

2. Cost aggregation

2.1 Smooth matching cost for all disparity values using Eq. (8&9).

2.2 Blocking artifacts are removed by median filter.

3. Disparity computation

3.1 After cost aggregation, disparity value corresponding to minimum cost constitutes the disparity map (Eq. 10).

4. Disparity refinement

4.1 Occluded pixels detected by left-right consistency check.

4.2 Occlusion filling is done by assigning minimum of left and right neighbor's disparity values.

4.3 Disparity map refinement by weighted median filter (Eq. 11).

Algorithm 1: Proposed algorithm for disparity map computation.

4 EXPERIMENTAL RESULTS

The proposed method is evaluated on Middlebury stereo datasets (Tsukuba, Venus, Teddy and Cones) [1], [25]. All the experimental results shown in this paper are

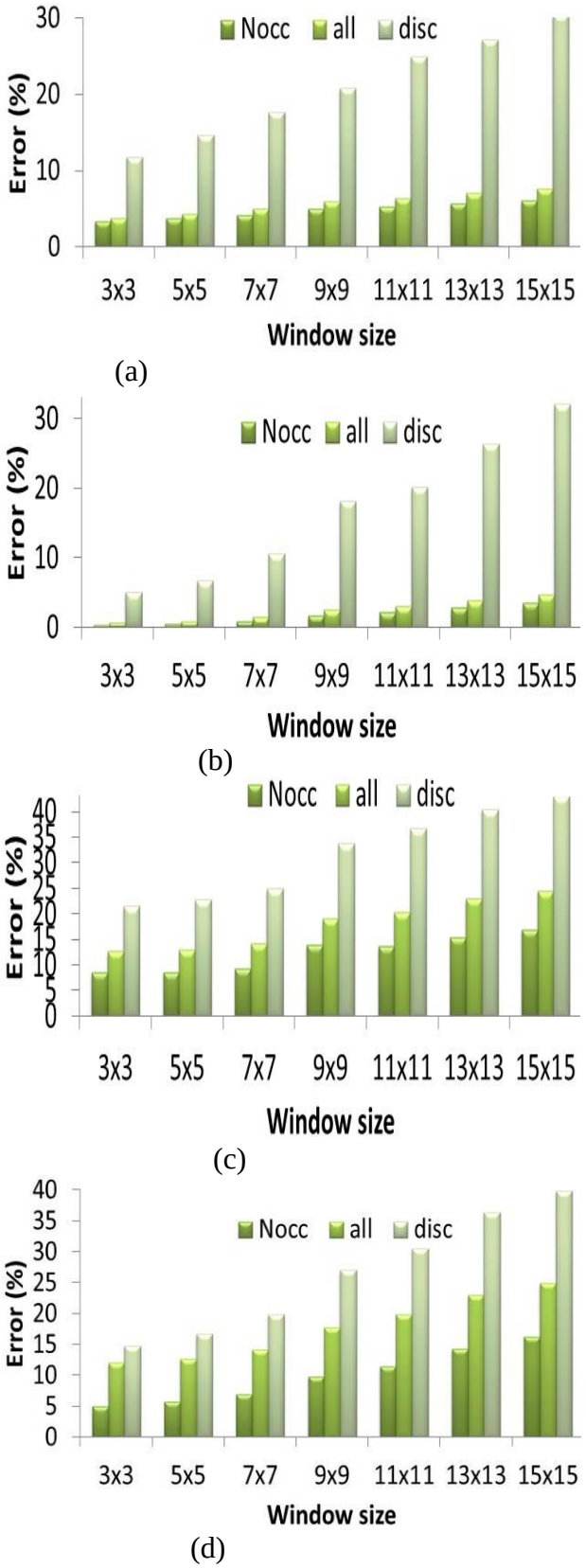

Figure 8. Variations of local stereo window size (a) Tsukuba, (b) Venus, (c) Teddy and (d) Cones.

evaluated for the error threshold of 1. In all the results shown, Nocc, all and disc represents the percentage of bad pixels (pixels having disparity values that deviates from the ground truth by +/- 1) in the nonoccluded region, entire image and discontinuities regions respectively. In order to show the effects of various parameters on the accuracy of the generated disparity map, the above experiment is repeated for different values of

- ❖ local stereo window size (SW);
- ❖ Kuwahara filter window size (KWS);
- ❖ median filter window size (MWS).

The experiment is also repeated for different numbers of

- ✓ principal components (PC);
- ✓ Gabor wavelet filter orientations (N_{theta});
- ✓ Gabor wavelet filter scaling (N_{scale})

Variation of local stereo window size: Figure 8 shows the percentage of errors (Nocc, all and disc) for different values of local stereo window for Tsukuba, Venus, Teddy and Cones images. The parameters used are: SW-starting from 3×3 to 15×15, KWS-9×9, MWS-3×3, % PC= 20%, N_{theta} = 2 and N_{scale} = 2. As the window size increases, there are more variations in the percentage of unwanted/bad pixels in the discontinuous regions compared to the non-occluded regions and the entire image. Figure 14(a) shows the average percentage of the bad pixels. The proposed method produces significantly good results even with a smallest window. This is due to that fact that the correlation of the pixels in the smaller window is more compared to the pixels in the larger window.

Variation of Kuwahara filter window size: The percentage of errors for Tsukuba, Venus, Teddy and Cones images are shown in Figure 9 for different Kuwahara filter window sizes. The parameters used are: SW-7×7, KWS-$5\times5, 9\times9, 13\times13, 17\times17$, 21×21 and 25×25, MWS-3×3, % PC= 20%, N_{theta} = 2 and N_{scale} = 2. In this case also, there are more variations

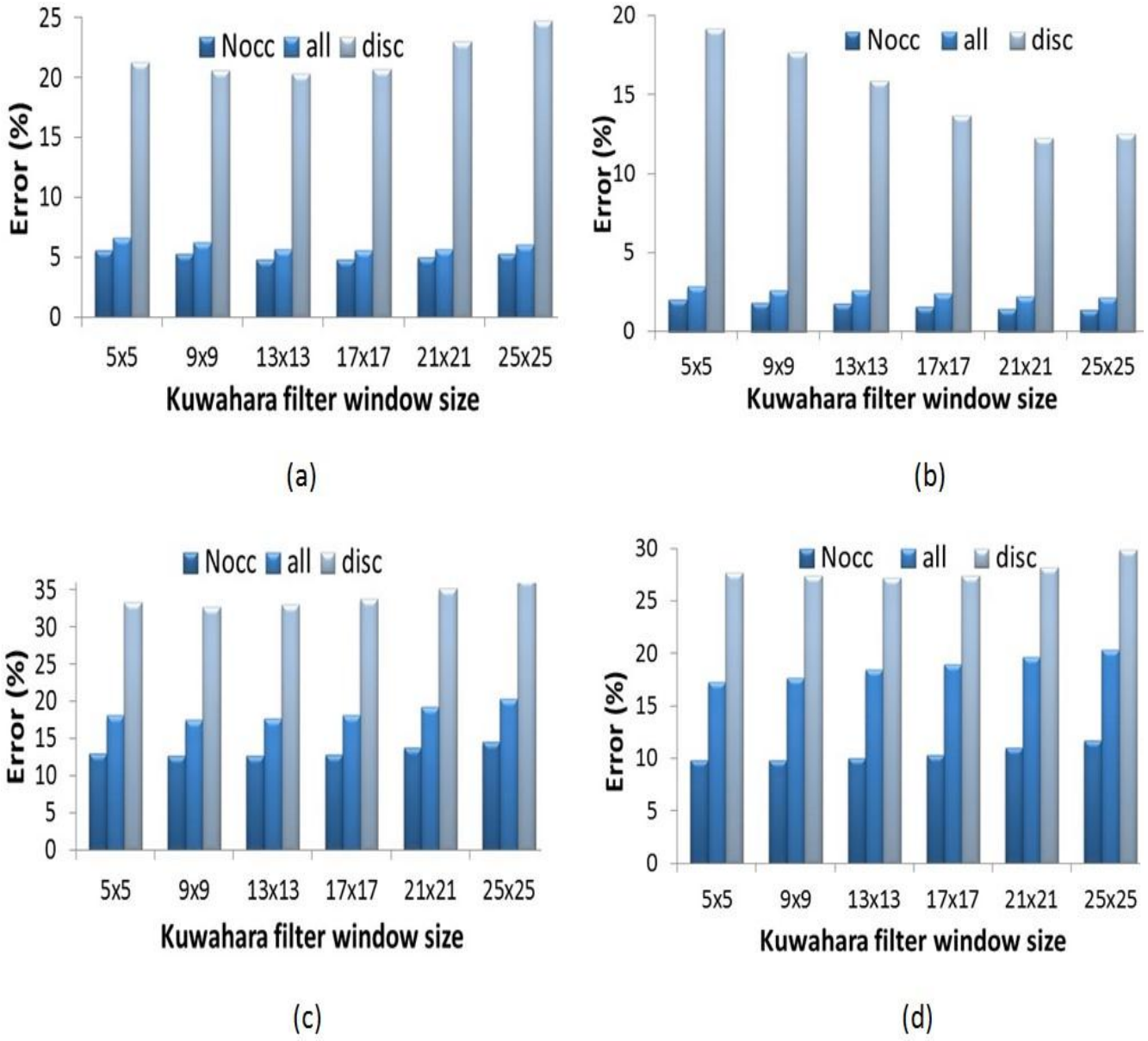

Figure 9. Variations of Kuwahara filter window size (a) Tsukuba, (b) Venus, (c) Teddy and (d) Cones.

in the percentage of unwanted/bad pixels for the bigger windows in the discontinuous regions compared to the non-occluded regions and the entire image. Figure 14(b) shows the average percentage of the bad pixels for different Kuwahara filter window sizes. It shows that a small window produces a detailed output image.

Variation of Median filter window size: Figure 10 shows the percentage of errors for different window sizes of the median filter. The parameters used are: SW- 3×3, KWS-5×5, MWS-starting from 3×3 to 15×15, % PC= 20%, N_{theta} = 2 and N_{scale} = 2. The average error percentage is shown in Figure 14(c). Similar to Kuwahara filter, a bigger median filter window blurs the edges, whereas a small median filter window retains the detailed information [26].

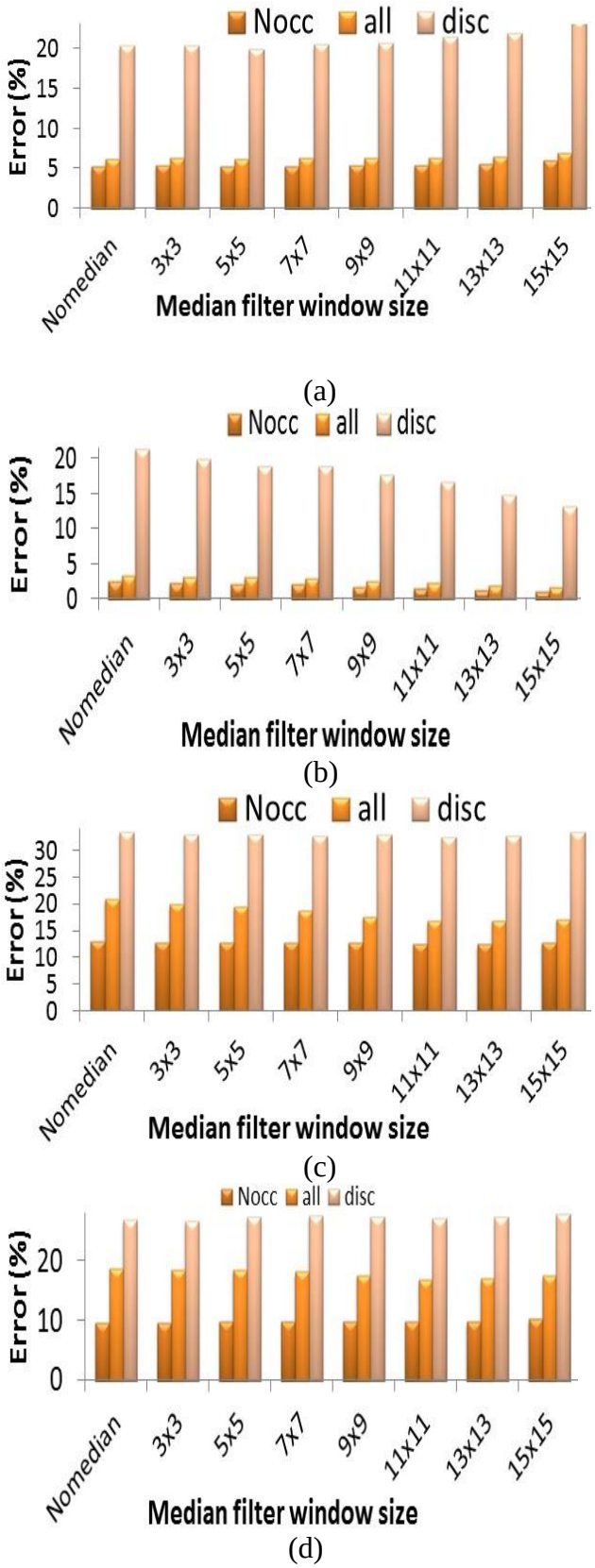

Figure 10. Variations of Median filter window size (a) Tsukuba, (b) Venus, (c) Teddy and (d) Cones.

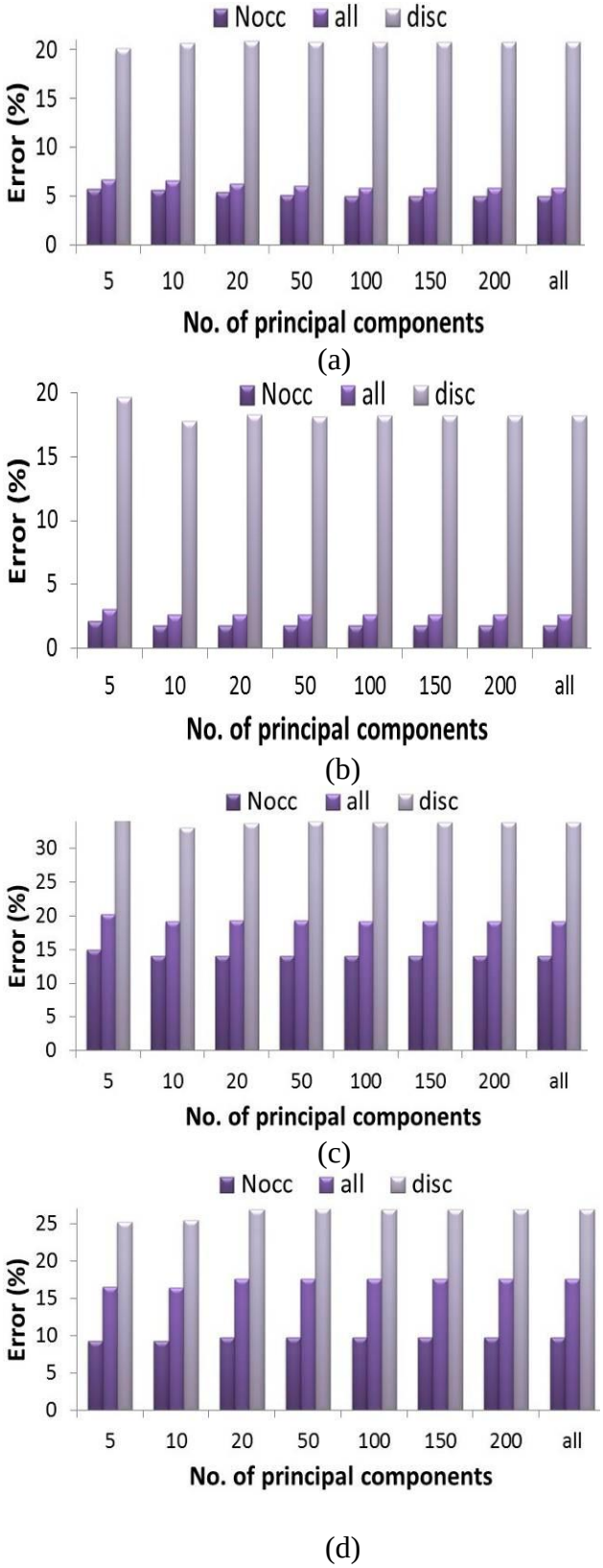

Figure 11. Variations of number of principal components. (a) Tsukuba, (b) Venus, (c) Teddy and (d) Cones.

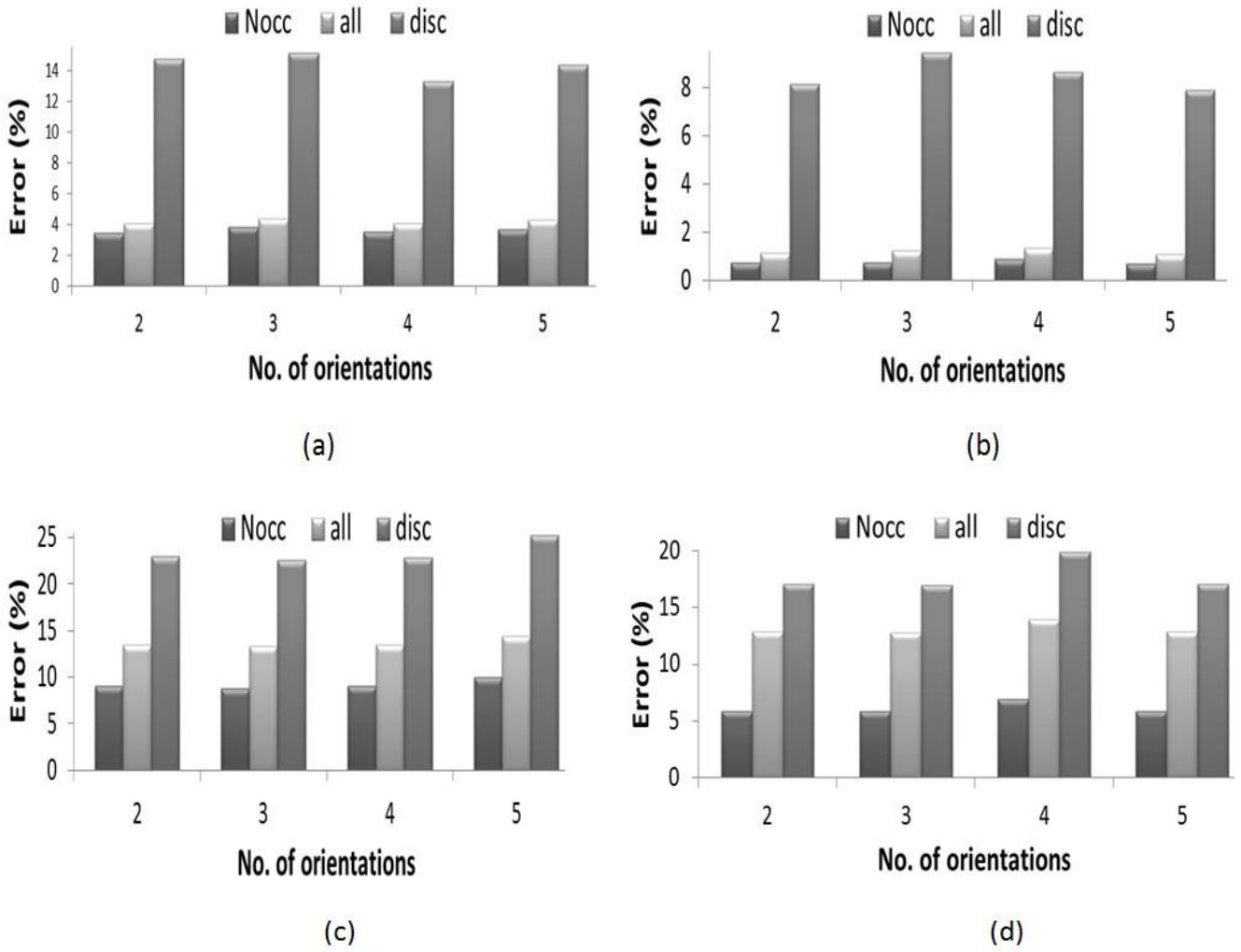

Figure 12. Variations of number of Gabor wavelet filter orientations. (a) Tsukuba, (b) Venus, (c) Teddy and (d) Cones.

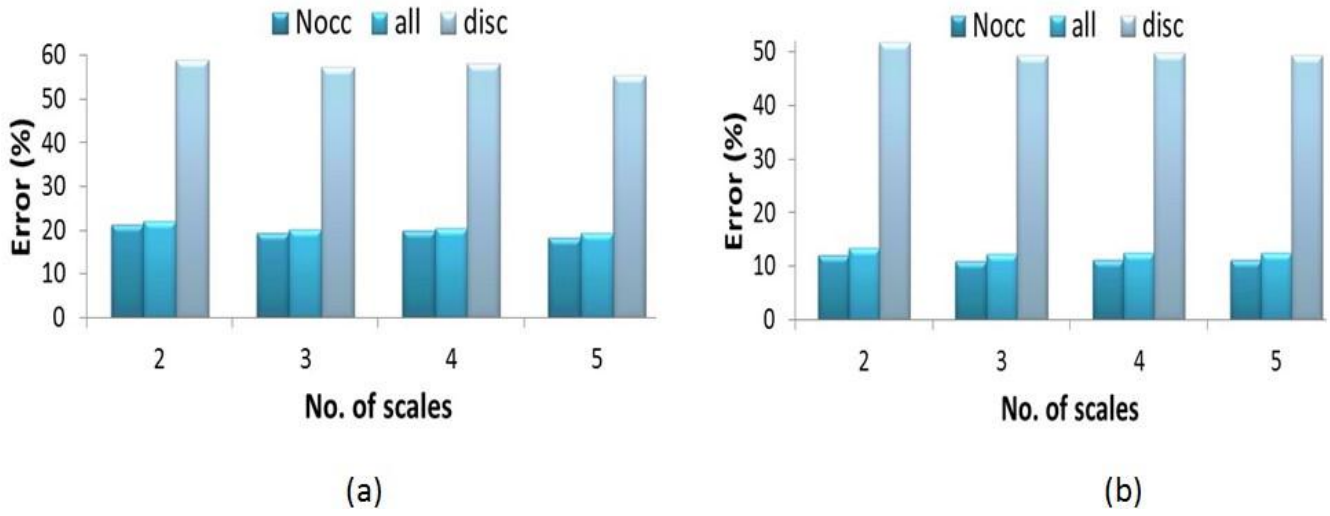

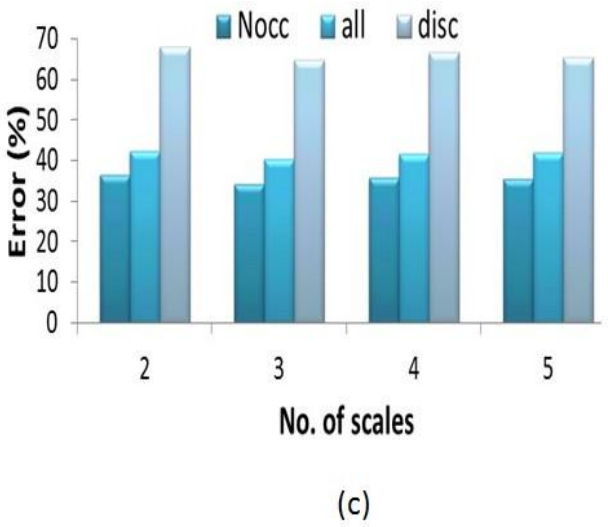

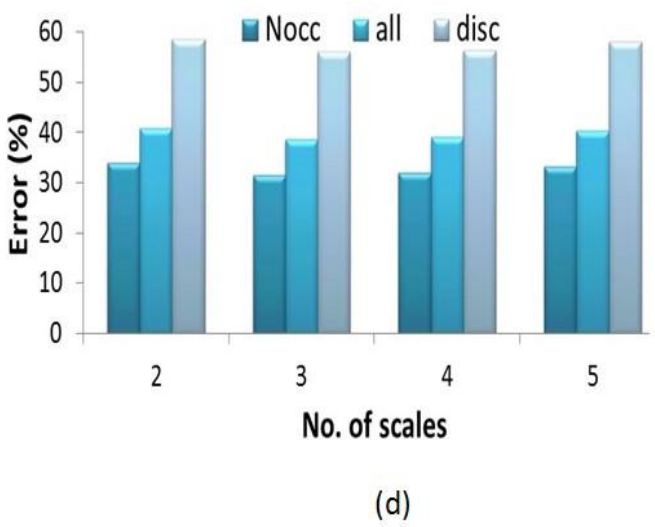

Figure 13. Variations of number of Gabor wavelet filter scaling. (a) Tsukuba, (b) Venus, (c) Teddy and (d) Cones.

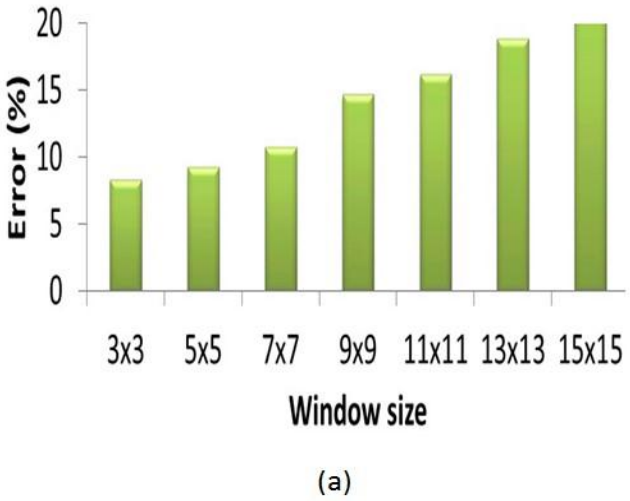

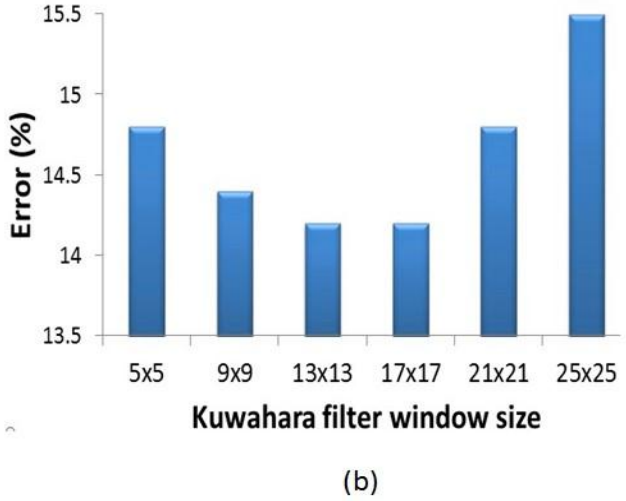

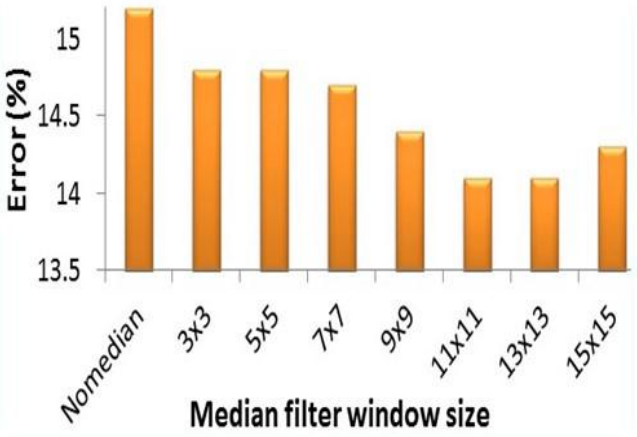

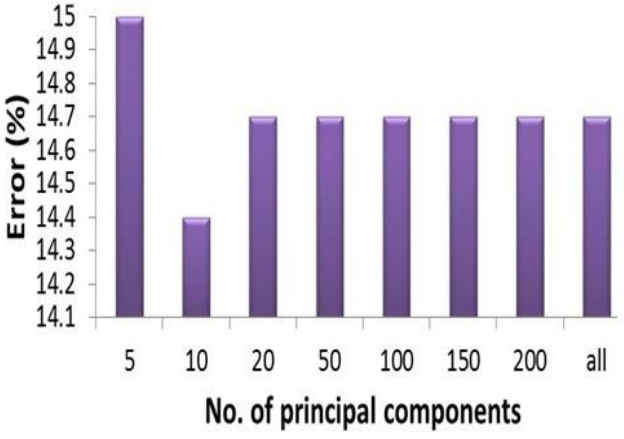

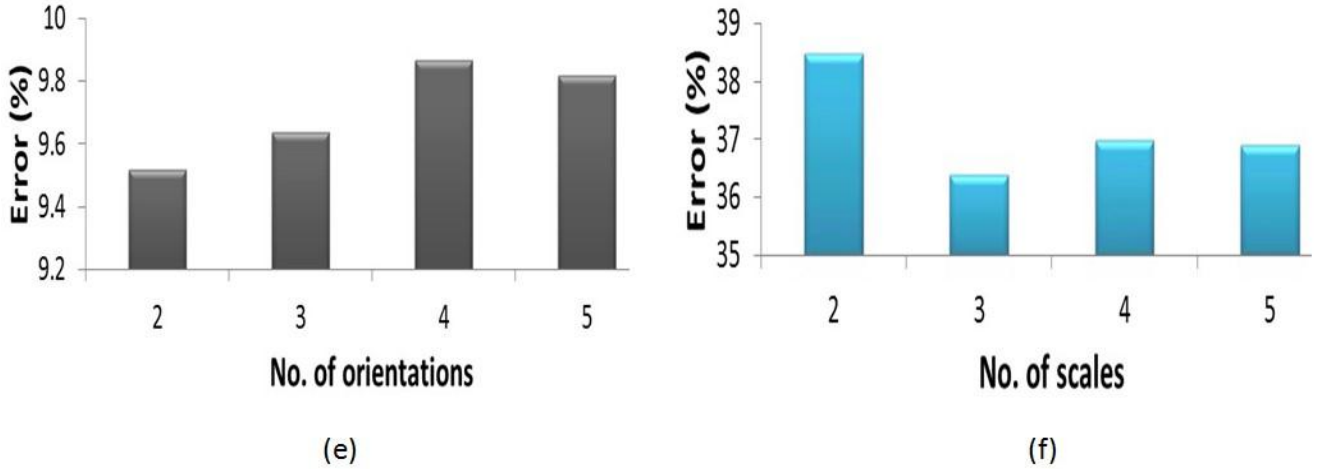

Figure 14. Average percentage of bad pixels. (a) Variation of local stereo window size, (b) Variation of Kuwahara filter window size, (c) Variation of Median filter window size, (d) Variation of number of principal components, (e) Number of Gabor wavelet filter orientations and (f) Number of Gabor wavelet filter scaling.

Variation of number of principal components: Figure 11 shows the percentage of errors for different numbers of principal components used for local stereo correspondences for all the four images of Middlebury datasets. The parameters used are: SW-9×9, KWS-5×5, MWS-3×3, no. of PC = 5, 10, 20, 50, 100, 150, 200 and all the coefficients, $N_{theta} = 2$ and $N_{scale} = 2$. Figure 11 shows that error is maximum for PC = 5 and it gradually decreases for PC = 10 and 20, after that the error does not increase significantly. Figure 14(d) shows the average percentage of bad pixels. When the Eigen values are arranged in the decreasing order, the principal components corresponding to the largest Eigen values contain more information [27]. Figure 11 and 14(d) shows that 20 principal components corresponding to the largest Eigen values contain most important information.

Variation of number of Gabor wavelet filter orientations: The percentage of errors for four Middlebury database images for different orientations of Gabor wavelet filter is shown in Figure 12. The parameters used are: SW-5×5, KWS-5×5, MWS-3×3, % PC= 20%, $N_{theta} = 2,3,4,5$ and $N_{scale} = 2$. It shows that the change in error is quite insignificant with respect to the number of orientations. Change in the average error for all the four images shown in Figure 14(e), which remains almost constant. This is due to the fact that the percentage of principal components remains same i.e., 20% of the total number of coefficients are used in this experiment.

Variation of number of Gabor wavelet filter scaling: Figure 13 shows the percentage of error for different numbers of filter scaling for all the four images of Middlebury datasets. The parameters used are: SW-33×33, KWS-5×5, MWS-3×3, % PC= 20%, $N_{theta} = 2$ and $N_{scale} = 2$, 3, 4 and 5. It is seen that error remains almost constant as the number of scaling increases. Apparently, Figure 14(f) shows that the average error is more for $N_{scale} = 2$ and then decreases for $N_{scale} = 3$; 4 and 5. In this case also, the change in error is quite insignificant. This is due to the fact that the percentage of principal components remains same i.e., 20% of the total number of coefficients are used in this experiment.

5 CONCLUSIONS

The maximum performance of the estimated disparity map is greatly influenced by the

selection of appropriate values for various parameters used. In this paper, we analyzed the impact of various parameters such as window size, number of principal components, number of Gabor filter orientations and scaling on the estimated disparity map and the reason behind it. This analysis helps us to choose the appropriate parameters to obtain accurate disparity map.

REFERENCES

[1] D. Scharstein and R. Szeliski, "A taxonomy and evaluation of dense two-frame stereo correspondence algorithms," Int'l J. Computer Vision, vol. 47, pp. 7-42, 2002.

[2] N. Lazaros, G. C. Sirakoulis and A. Gasteratos, "Review of stereo vision algorithms: From software to hardware," Int'l J. Optomechatronics, vol. 2, pp. 435-462, 2008.

[3] T. Ndhlovu, "An investigation into stereo algorithms: An emphasis on local-matching," MSc. dissertation, Dept. Elec. Engg, Univ. of Cape Town, Cape Town, 2011.

[4] H. Hirschmuller, M. Buder and I. Ernst, "Stereo processing by semiglobal matching and mutual information," IEEE Trans. Pattern Anal. Mach. Intell., vol. 30, pp. 328-341, 2008.

[5] M. Z. Brown, D. Burschka and G. D. Hager, "Advances in Computational Stereo," IEEE Trans. Pattern Analysis and Machine Intelligence, vol. 25, pp. 993-1008, 2003.

[6] R. Zabih and J. Woodfill, "Non-parametric Local Transforms for Computing Visual Correspondence," European Conf. on Computer Vision, 1994, pp. 151-158.

[7] C. C. Pham, V. D. Nguyen and J. W. Jeon, "Efficient spatio-temporal local stereo matching using information permeability filtering," IEEE Int. Conf. on Image Processing, 2012, pp. 2965-2968.

[8] K. J. Yoon and I. S. Kweon, "Adaptive support-weight approach for correspondence search," IEEE Trans. Pattern Anal. Mach. Intell., vol. 28, pp. 650-656, 2006.

[9] A. Hosni, M. Bleyer and M. Gelautz, "Secrets of adaptive support weight techniques for local stereo matching," Comput. Vision and Image Understand., vol. 117, pp. 620-632, 2013.

[10] M. Gerrits and P. Bekaert, "Local stereo matching with segmentation-based outlier rejection," Candian Conf. Computer and Robot Vision, 2006.

[11] A. Hosni, M. Bleyer, M. Gelautz, C. Rhemann, "Local stereo matching using geodesic support weights," Int'l Conf. Image Processing, 2009, pp. 2093–2096.

[12] K. Zhang, Y. Fang, D. Min, L. Sun, S. Y. Yan, Q. Tian, et al. Cross-scale cost aggregation for stereo matching. Int'l Conf. Computer Vision and Pattern Recognition, 2014.

[13] K. Zhang, J. Lu and G. Lafruit, "Cross-based local stereo matching using orthogonal integral images," IEEE Trans. Circuits Syst. Video Technol., vol. 19, pp. 1073–1079, 2009.

[14] C. Cigla, A.A. Alatan, Efficient edge-preserving stereo matching, Int'l Conf. Computer Vision Workshops, 2011, pp. 696–699.

[15] A. Hosni, C. Rhemann, M. Bleyer, C. Rother, and M. Gelautz, "Fast cost-volume filtering for visual correspondence and beyond," IEEE Trans. Pattern Anal. Mach. Intell.,vol. 35, pp. 504-511, 2013.

[16] D. Min, J. Lu and M. N. Do, "Joint Histogram-Based Cost Aggregation for Stereo Matching,. IEEE Trans. Pattern Anal. Mach. Intell., vol. 35, 2539-2545, 2013.

[17] C. C. Pham and J. W. Jeon, "Domain Transformation-Based Efficient Cost Aggregation for Local Stereo Matching," IEEE Trans. Circuits Syst. Video Techn., vol. 23, pp. 1119-1130, 2013.

[18] T. S. Lee, "Image representation using 2D Gabor wavelets," IEEE Trans. Pattern Anal. Mach. Intell., vol. 18, pp. 959-971, 1996.

[19] J. G. Daugman, "Uncertainty relation for resolution in space, spatial frequency and orientation optimized by two-dimensional visual cortical filters," Journal of the Optical Society of America A, vol. 2, pp. 1160-1169, 1985.

[20] S. Bhagavathy, J. Tesic and B. S. Manjunath, "On the Rayleigh nature of Gabor filter outputs," IEEE Int. Conf. on Image Processing, 2003, pp. 745-748.

[21] M. K. Bhuyan and Malathi. T, "Review of the Application of Matrix Information Theory in Video Surveillance,"in Matrix Information Geometry, Frank Nielsen and Rajendra Bhatia, Ed. Springer, 2012, pp.293-321.

[22] G. Papari, N. Petkov and P. Campisi, "Artistic Edge and Corner Enhancing Smoothing," IEEE Trans. Image Processing, vol. 16, pp. 2449-2461, 2007.

[23] A. Hosni, M. Bleyer, M. Gelautz and C. Rhemann, "Local Stereo Matching Using Geodesic Support Weights," Int'l Conf. Image Processing, 2009, pp. 2093-2096.

[24] Z. Ma, K. He, Y. Wei, J. Sun and E. Wu, "Constant Time Weighted Median Filtering for Stereo Matching and Beyond," Int'l Conf. Computer Vision and Pattern Recognition, 2013, pp. 1-8.

[25] D. Scharstein and R. Szeliski, "High-accuracy stereo depth maps using structured light," Int'l Conf. Computer Vision and Pattern Recognition, 2003, pp. 195-202.

[26] S. Jayaraman, S. Esakkirajan and T. Veerakumar. Digital Image Processing. Tata McGraw Hill, 2009.

[27] R. C. Gonzalez and R. E. Woods. Digital Image Processing. Pearson Education, 2008, pp. 864-974.